
DISENTANGLED REPRESENTATION LEARNING AND GENERATION WITH MANIFOLD OPTIMIZATION

Arun Pandey

Department of Electrical Engineering
ESAT-STADIUS, KU Leuven
Kasteelpark Arenberg 10, B-3001 Leuven, Belgium
arun.pandey@esat.kuleuven.be

Michaël Fanuel

Department of Electrical Engineering
ESAT-STADIUS, KU Leuven
Kasteelpark Arenberg 10, B-3001 Leuven, Belgium
michael.fanuel@esat.kuleuven.be

Joachim Schreurs

Department of Electrical Engineering
ESAT-STADIUS, KU Leuven
Kasteelpark Arenberg 10, B-3001 Leuven, Belgium
joachim.schreurs@esat.kuleuven.be

Johan A. K. Suykens

Department of Electrical Engineering
ESAT-STADIUS, KU Leuven
Kasteelpark Arenberg 10, B-3001 Leuven, Belgium
johan.suykens@esat.kuleuven.be

November 25, 2021

ABSTRACT

Disentanglement is an enjoyable property in representation learning which increases the interpretability of generative models such as Variational Auto-Encoders (VAE), Generative Adversarial Models and their many variants. In the context of latent space models, this work presents a representation learning framework that explicitly promotes disentanglement thanks to the combination of an auto-encoder with Principal Component Analysis (PCA) in latent space. The proposed objective is the sum of an auto-encoder error term along with a PCA reconstruction error in the feature space. This has an interpretation of a Restricted Kernel Machine with an interconnection matrix on the Stiefel manifold. The construction encourages a matching between the principal directions in latent space and the directions of orthogonal variation in data space. The training algorithm involves a stochastic optimization method on the Stiefel manifold, which increases only marginally the computing time compared to an analogous VAE. Our theoretical discussion and various experiments show that the proposed model improves over many VAE variants along with special emphasis on disentanglement learning.

1 Introduction

Latent space models are popular tools for sampling from high dimensional distributions. Often, only a small number of latent factors is sufficient to describe data variations. These models exploit the underlying structure of the data and learn explicit representations that are faithful to data generative factors. Popular latent space models are Variational Auto-Encoders (VAEs) [12], Restricted Boltzmann Machines (RBMs) [26], Normalizing flows [24] and their many variants. In latent variable modelling, one is often interested in modelling the data in terms of *uncorrelated* or *independent* components, yielding a so-called ‘disentangled’ representation [1] which are often studied in the context of VAEs (see Figure 1). An advantage of such a representation is that the different latent units impart more interpretability to the model. One popular variant achieving disentanglement is the β -VAE [9], that we describe shortly hereafter.

Let $p(\mathbf{x})$ be the distribution of the data $\mathbf{x} \in \mathbb{R}^d$ and consider latent vectors $\mathbf{z} \in \mathbb{R}^\ell$ with $p(\mathbf{z})$ its prior distribution, chosen to be a standard normal. Then, one defines an encoder $q(\mathbf{z}|\mathbf{x})$ that can be deterministic or random, e.g. given by $\mathcal{N}(\mathbf{z}|\phi(\mathbf{x}), \gamma^2\mathbb{I})$, where the mean and variance are parameterized as a neural network ϕ . A random decoder $p(\mathbf{x}|\mathbf{z}) = \mathcal{N}(\mathbf{x}|\psi(\mathbf{z}), \sigma_0^2\mathbb{I})$ is associated to the decoder neural network ψ which maps latent codes to data points. The



Figure 1: Latent traversals along the first principal component from a trained St-RKM model on 3Dshapes (left) and Dsprites (right) dataset. The latent coordinate clearly isolates the floor colour and scale respectively without entangling with any other factor.

VAEs are originally estimated by maximizing the lower bound

$$\mathbb{E}_{\mathbf{z} \sim q(\mathbf{z}|\mathbf{x})}[\log(p(\mathbf{x}|\mathbf{z}))] - \beta \text{KL}(q(\mathbf{z}|\mathbf{x}), p(\mathbf{z})) \leq \log p(\mathbf{x}), \quad (1)$$

which is called the Evidence Lower Bound (ELBO) when $\beta = 1$. It has been argued that the Kullback-Liebler (KL) divergence term in the ELBO is responsible for the disentanglement of the representation, while larger values of $\beta > 1$ promote more disentanglement [9].

To introduce the model proposed in this paper, we firstly make explicit the connection between β -VAEs and standard Auto-Encoders (AEs). Let the dataset be $\{\mathbf{x}_i\}_{i=1}^n$ with $\mathbf{x}_i \in \mathbb{R}^d$. If we assume an encoder $q(\mathbf{z}|\mathbf{x}) = \mathcal{N}(\mathbf{z}|\phi(\mathbf{x}), \gamma^2\mathbb{I})$ with $\mathbf{z} \in \mathbb{R}^\ell$ and for a fixed $\gamma > 0$, the maximization problem (1) is then equivalent to the minimization of the ‘regularized’ AE

$$\frac{1}{n} \sum_{i=1}^n \left\{ \frac{1}{2\sigma_0^2} \mathbb{E}_{\epsilon \sim \mathcal{N}(0, \mathbb{I})} \|\mathbf{x}_i - \psi(\phi(\mathbf{x}_i) + \gamma\epsilon)\|_2^2 + \frac{\beta}{2} \|\phi(\mathbf{x}_i)\|_2^2 \right\}, \quad (2)$$

where additive constants depending on γ have been omitted. In this paper, we consider a latent space model based on the variant of Restricted Kernel Machines (RKM) [28] formulation, which can be interpreted as adding the RKM objective function to the AE objective of the form (2) with $\gamma \approx 0$. RKMs yield a representation of kernel methods with visible and hidden units establishing links between Kernel Principal Component Analysis (KPCA) and RBMs. This framework has an energy form similar to RBM [14] and there is a training procedure in a non-probabilistic setting. In this paper, we consider the RKM associated to the optimization problem

$$\min_{\|U\|_F \leq C} \min_{\mathbf{h}_i \in \mathbb{R}^m} \sum_{i=1}^n \left\{ \underbrace{-\phi(\mathbf{x}_i)^\top U \mathbf{h}_i + f(\mathbf{h}_i)}_{\text{RKM}} + L_U(\mathbf{x}_i, \phi(\mathbf{x}_i)) \right\} \quad (3)$$

where $\phi(\mathbf{x}_i) \in \mathbb{R}^\ell$, $\mathbf{h}_i \in \mathbb{R}^m$ with $m \leq \ell$ and U is an interconnection matrix¹. The function $f: \mathbb{R}^m \rightarrow]-\infty, +\infty]$ is used for regularization and can for instance be chosen as closed and strongly convex, or as the characteristic function of a closed set. The additional term L_U is a reconstruction loss such as (2), that we define precisely in the next section. The analogy with RBM goes as follows: $\phi(\mathbf{x}_i)$ is interpreted as visible ‘units’ whereas U plays the role of an interconnection matrix with hidden features \mathbf{h}_i . These ‘relaxed’ hidden units are not binary valued contrary to RBMs. The minimization over \mathbf{h}_i yields the first term of the optimal objective $-f^*(U^\top \phi(\mathbf{x}_i))$ in terms of the Fenchel conjugate of f . Two simple examples are the following:

- $f(\mathbf{h}) = \frac{1}{2} \|\mathbf{h}\|_2^2$ yielding a PCA interpretation with $\mathbf{h}_i^* = U^\top \phi(\mathbf{x}_i)$, as explained hereafter,
- $f(\mathbf{h}) = \chi_{\mathbb{S}^{m-1}}(\mathbf{h})$ corresponding to spherical units with $\mathbf{h}_i^* = U^\top \phi(\mathbf{x}_i) / \|U^\top \phi(\mathbf{x}_i)\|_2$.

In this paper, we focus mainly on the squared norm regularizer, while spherical units are briefly described in supplementary material.

Contributions: We propose two main changes with respect to related works: (i) The interconnection matrix U is restricted to be a rectangular matrix with orthonormal columns, i.e., valued on a Stiefel manifold. Then, for the training, we utilize the Cayley ADAM algorithm of [15] for stochastic optimization on the Stiefel manifold, where we call our proposed model St-RKM. From the computational viewpoint, the proposed method only increases the training time by a reasonably small amount compared with β -VAEs for instance. To the best of our knowledge, manifold optimization has not been previously explored in the context of disentangled representation learning. (ii) We propose several Auto-Encoder objectives to learn the feature map and the pre-image map networks in the form of an encoder and a decoder respectively. We argue that the combination of a stochastic AE loss with an explicit optimization on the Stiefel manifold promotes disentanglement. (iii) Further we establish connections with probabilistic models, formulate an Evidence-Lower Bound (ELBO) and discuss independence of latent factors. Experiments illustrate the merit of proposed method by improving over many variants of VAEs.

¹In [28], the constraint on U is implemented as a soft penalty term.

Related work: VAE. It has been shown in [4] that the KL term includes the Mutual Information Gap - which encourages disentanglement. In [3], the effect of the β term is analyzed more in depth. It was suggested that the stronger pressure for the posterior to match the factorised unit Gaussian prior puts extra constraints on the implicit capacity of the latent bottleneck [9]. Recently, several variants of VAEs promoting disentanglement have been proposed by adding extra terms to the ELBO. For instance, FactorVAE [11] augments the ELBO by a new term enforcing factorization of the marginal posterior (or aggregate posterior). A comprehensive study on disentanglement and many VAE variants is done in [16]. Recently, another work [17] considers adding an extra term which accounts for the knowledge of some partial label information in order to improve disentanglement. In [25] the reason for the alignment of the latent space with the coordinate axes is analyzed, as the design of the VAE does not suggest any such mechanism. The authors argue that due to the diagonal approximation in the encoder together with the inherent stochasticity forces the local orthogonality of the decoder. This local behavior of promoting both reconstruction and orthogonality matches closely how the PCA embedding is chosen. Experiments show that VAEs indeed strive for local orthogonality, and there is a clear correlation between orthogonality and the disentanglement score. In contrast to [25] where implicit orthogonality of VAEs is studied, our proposed model has orthogonality by design due to the introduction of Stiefel manifold. The use of deterministic AEs was studied in [7]. The authors argue that sampling a stochastic encoder in a Gaussian VAE can be interpreted as simply injecting noise to the input of a deterministic decoder. Further, they propose a similar quadratic regularization on the latent vectors: $\frac{1}{2}\|z\|_2^2$ as was proposed in the original RKM formulation [28]; and achieve generation by a post density estimation step using a Gaussian mixture model. Compared to [7], we go one step further by introducing the Stiefel manifold, combining it with the insights gained in [25].

RKM. In [21] for instance, a multi-view generative model called Generative-RKM (Gen-RKM) has been introduced which uses explicit feature-maps in a novel training procedure for joint feature-selection and subspace learning. In this work, the feature map ϕ_θ is a neural network parametrized by θ . Then, a transposed convolutional neural network [5] can be used for the pre-image map ψ_ζ parametrized by ζ . Alternatively, the feature map ϕ can be associated with a positive semi-definite kernel such that $k(\mathbf{x}, \mathbf{y}) = \langle \phi(\mathbf{x}), \phi(\mathbf{y}) \rangle_{\ell^2}$, such as the Gaussian RBF kernel for which pre-image problems have been studied [27]. Gen-RKM learns a basis of low-dimensional latent space which makes it possible to generate data with specific characteristics, i.e. a disentangled representation. Further, [22] proposed a mechanism for robustness in Gen-RKM using a weighting function based on Minimum Covariance Determinant.

2 Proposed method

Our initial optimization problem is derived from (3) with squared norm regularizer and with interconnection matrix $U = [\mathbf{u}_1 \dots \mathbf{u}_m]$ belonging to the Stiefel manifold $\text{St}(\ell, m)$, that is, the set of $\ell \times m$ matrices with orthonormal columns ($\ell \geq m$). It is given by

$$\min_{\theta, \xi} \min_{U \in \text{St}(\ell, m)} \min_{\mathbf{h}_i \in \mathbb{R}^m} \sum_{i=1}^n \left\{ \|\mathbf{h}_i\|_2^2 - 2\phi_\theta^\top(\mathbf{x}_i)U\mathbf{h}_i + \|\phi_\theta(\mathbf{x}_i)\|_2^2 + \lambda L_{\xi, U}(\mathbf{x}_i, \phi_\theta(\mathbf{x}_i)) \right\}, \quad (4)$$

with θ, ξ denoting real-valued parameter vectors and $\lambda > 0$. The feature map is also assumed to be centered, i.e. $\mathbb{E}_{\mathbf{x} \sim p(\mathbf{x})}[\phi_\theta(\mathbf{x})] = \mathbf{0}$. The idea consists in learning an auto-encoder together with an ‘optimal’ linear subspace of the latent space generated by the columns of U , whose projector is $\mathbb{P}_U = UU^\top$. Namely, we define an AE loss:

$$L_{\xi, U}^{(\sigma)}(\mathbf{x}, \mathbf{z}) = \mathbb{E}_{\epsilon \sim \mathcal{N}(0, \mathbb{I}_m)} \|\mathbf{x} - \psi_\xi(\mathbb{P}_U \mathbf{z} + \sigma U \epsilon)\|_2^2, \quad (5)$$

which is deterministic for $\sigma = 0$. The noise term $\sigma U \epsilon$ in (5) is promoting a *smoother* decoder network. The second loss we propose is a splitted AE loss

$$L_{\xi, U}^{(\sigma), sl}(\mathbf{x}, \mathbf{z}) = L_{\xi, U}^{(0)}(\mathbf{x}, \mathbf{z}) + \mathbb{E}_{\epsilon \sim \mathcal{N}(0, \mathbb{I}_m)} \|\psi_\xi(\mathbb{P}_U \mathbf{z}) - \psi_\xi(\mathbb{P}_U \mathbf{z} + \sigma U \epsilon)\|_2^2, \quad (6)$$

where the first term is the classical AE loss while the second term promotes orthogonal directions of variations and is related to the Lemma 1 below.

2.1 Subspace learning.

By minimizing first over \mathbf{h}_i in (4), we find the score vector $\mathbf{h}_i^* = U^\top \phi_\theta(\mathbf{x}_i)$ with respect to the columns of U , the orthonormal set $\{\mathbf{u}_1, \dots, \mathbf{u}_m\}$. After substitution, the optimization problem is:

$$\min_{\theta, \xi} \min_{U \in \text{St}(\ell, m)} \frac{1}{n} \sum_{i=1}^n \left\{ \|\mathbb{P}_{U^\perp} \phi_\theta(\mathbf{x}_i)\|_2^2 + \lambda L_{\xi, U}(\mathbf{x}_i, \phi_\theta(\mathbf{x}_i)) \right\}. \quad (7)$$

Table 1: FID Scores [8] on 10 runs for 8000 randomly generated samples. The Sliced Wasserstein Distance (SWD) scores are in the supplementary material. (smaller is better).

Models	MNIST	fMNIST	SVHN	Dsprites	3Dshapes	Cars3D
St-RKM ($\sigma = 0$)	28.71 (± 0.33)	67.70 (± 0.50)	62.97 (± 0.34)	88.82 (± 1.32)	25.76 (± 1.74)	174.42 (± 0.32)
St-RKM ($\sigma = 10^{-3}$)	28.83 (± 0.23)	66.84 (± 0.28)	60.42 (± 0.32)	84.91 (± 1.81)	21.87 (± 0.18)	169.86 (± 0.44)
St-RKM-sl ($\sigma = 10^{-3}$)	28.58 (± 0.21)	73.85 (± 0.36)	60.40 (± 0.34)	75.94 (± 0.82)	23.14 (± 0.38)	174.76 (± 0.52)
VAE ($\beta = 1$)	39.38 (± 0.31)	101.26 (± 0.54)	71.13 (± 0.36)	119.55 (± 1.46)	37.62 (± 1.63)	213.09 (± 0.30)
β -VAE ($\beta = 3$)	30.14 (± 0.19)	86.12 (± 0.62)	72.93 (± 0.47)	83.25 (± 1.87)	30.39 (± 1.01)	172.39 (± 0.41)
FactorVAE	35.12 (± 1.32)	91.43 (± 2.16)	87.45 (± 1.4)	61.83 (± 1.23)	41.45 (± 1.66)	175.21 (± 0.22)
Info-GAN	77.75 (± 2.05)	78.77 (± 12.51)	98.10 (± 1.21)	121.46 (± 2.84)	55.11 (± 3.18)	177.14 (± 0.21)

The orthonormal vectors $\{\mathbf{u}_1, \dots, \mathbf{u}_m\}$ provides directions associated to different generative factors of our generative model. Notice that what we propose is not simply another encoder architecture. Namely, in view of the AE loss, one could argue that we simply consider a special choice of encoder and decoder: $U^\top \phi_\theta(\cdot)$ and $\psi_\xi(U \cdot)$. However, the optimization of the parameters in the last layer of the encoder does not play a redundant role with the optimization over U^\top , since the first term in (7) clearly also depends on $\mathbb{P}_{U^\perp} \phi_\theta(\cdot)$. In other words, our objective assumes that the neural network defining the encoder provides a better embedding if we impose that it maps training points on a linear subspace of dimension m in the ℓ -dimensional latent space. The PCA interpretation is clear if we introduce the covariance matrix $C_\theta = \frac{1}{n} \sum_{i=1}^n \phi_\theta(\mathbf{x}_i) \phi_\theta^\top(\mathbf{x}_i)$. Then, the first term in (7) $\frac{1}{n} \sum_{i=1}^n \|\mathbb{P}_{U^\perp} \phi_\theta(\mathbf{x}_i)\|_2^2$ can be written as $\text{Tr}(C_\theta - \mathbb{P}_U C_\theta \mathbb{P}_U)$. This corresponds to the reconstruction error of Kernel PCA, for the kernel $k_\theta(\mathbf{x}, \mathbf{y}) = \phi_\theta^\top(\mathbf{x}) \phi_\theta(\mathbf{y})$. Clearly, if \mathbb{P}_U is the projector on the m principal components, then $U^\top C_\theta U = \text{diag}(\boldsymbol{\lambda})$, where $\boldsymbol{\lambda}$ is a vector containing the principal values.

2.2 Decoder smoothness and disentanglement

In the case of the stochastic loss, the smoothness of the decoder is motivated by the following Lemma which extends the result of [25] and is adapted to the context of optimization on the Stiefel manifold.

Lemma 1 *Let $\boldsymbol{\epsilon} \sim \mathcal{N}(\mathbf{0}, \mathbb{I}_m)$ a random vector and $U \in \text{St}(\ell, m)$. Let $\psi_a(\cdot) \in \mathcal{C}^2(\mathbb{R}^\ell)$ with $a \in [d]$. If the function $[\psi(\cdot) - \mathbf{x}]_a^2$ has L -Lipschitz continuous Hessian, we have*

$$\begin{aligned} \mathbb{E}_\epsilon [\mathbf{x} - \psi(\mathbf{y} + \sigma U \boldsymbol{\epsilon})]_a^2 &= [\mathbf{x} - \psi(\mathbf{y})]_a^2 + \sigma^2 \text{Tr}(U^\top \nabla \psi_a(\mathbf{y}) \nabla \psi_a(\mathbf{y})^\top U) \\ &\quad - \sigma^2 [\mathbf{x} - \psi(\mathbf{y})]_a \text{Tr}(U^\top \text{Hess}_\mathbf{y}[\psi_a] U) + R_a(\sigma), \end{aligned} \quad (8)$$

with $|R_a(\sigma)| \leq \frac{1}{6} \sigma^3 L \frac{\sqrt{2(m+1)} \Gamma((m+1)/2)}{\Gamma(m/2)}$ where Γ is Euler's Gamma function.

In Lemma 1, the extra terms proportional to σ^2 can be interpreted as biases. Specifically, the second term on the RHS of (8) indicates that the stochastic AE loss tends to promote a smooth decoder. Strikingly, minimizing the second term encourages a small directional derivative in the directions given by $\{\mathbf{u}_1, \dots, \mathbf{u}_m\}$.

Disentanglement. Here we argue that *the principal directions in latent space are required to match orthogonal directions of variation in the data space* – the disentanglement of our representation is due to the optimization over $U \in \text{St}(\ell, m)$ and promoted by the stochastic AE loss. Let $\boldsymbol{\Delta}_\ell = \nabla \psi(\mathbf{y})^\top \mathbf{u}_\ell$ and $t \in \mathbb{R}$. Denote by $\boldsymbol{\Delta}$ the matrix with $\boldsymbol{\Delta}_\ell$ as columns. Then, as one moves from \mathbf{y} in the latent space in the direction of \mathbf{u}_ℓ , the generated data changes by

$$\psi(\mathbf{y} + t \mathbf{u}_\ell) - \psi(\mathbf{y}) = t \boldsymbol{\Delta}_\ell + \mathcal{O}(t^2).$$

Consider now a different direction, i.e., $\ell \neq \ell'$, and recall that \mathbf{u}_ℓ and $\mathbf{u}_{\ell'}$ are orthogonal. A disentangled representation would satisfy: $\boldsymbol{\Delta}_\ell^\top \boldsymbol{\Delta}_{\ell'} = 0$. In other words, as the latent point moves along \mathbf{u}_ℓ or along $\mathbf{u}_{\ell'}$, the decoder output varies in significantly different manner. Hence, for all \mathbf{y} in the latent space, we expect the Gram matrix $\boldsymbol{\Delta}^\top \boldsymbol{\Delta}$ to be diagonal. Now, we address the important role of the optimization problem. In the sequel, we assume abusively that the argument of the decoder is $\mathbf{y}_i = U U^\top \phi_\theta(\mathbf{x}_i) \approx \phi_\theta(\mathbf{x}_i)$. This approximation allows us to isolate the connection between (8) and the disentanglement of the representation. Then, coming back to Lemma 1, we observe that the stochastic AE objective includes diagonalization terms involving the trace of a symmetric matrix. Then, we rely on Proposition 1 whose proof is straightforward.

Proposition 1 *Let M be a $\ell \times \ell$ symmetric matrix with distinct eigenvalues. Let ν_1, \dots, ν_m be its m smallest eigenvalues, with the associated eigenvectors $\mathbf{v}_1, \dots, \mathbf{v}_m$. Let V be the matrix whose columns are these eigenvectors. Then, the optimization problem $\min_{U \in \text{St}(\ell, m)} \text{Tr}(U^\top M U)$ is solved by $U^* = V$ and we have $U^{*\top} M U^* = \text{diag}(\boldsymbol{\nu})$, with $\boldsymbol{\nu} = (\nu_1, \dots, \nu_m)^\top$.*

If we consider only the second term in (8) and take $M_i = \nabla\psi(\mathbf{y}_i)\nabla\psi(\mathbf{y}_i)^\top$, we see, thanks to Proposition 1, that the optimization over $U \in \text{St}(\ell, m)$ promotes a diagonal Gram matrix $\Delta\Delta^\top = U^\top M_i U$. By construction, the loss (6) does not include the third term in (8). Hence, considering also the first term in (7), we observe that the optimization over U promotes a matching between principal components and orthogonal directions of variation, as can be seen in

$$\min_{U \in \text{St}(\ell, m)} \frac{1}{n} \sum_{i=1}^n \text{Tr} \left[U^\top (\sigma^2 \nabla\psi_\xi(\phi_\theta(\mathbf{x}_i)) \nabla\psi_\xi(\phi_\theta(\mathbf{x}_i))^\top - \phi_\theta(\mathbf{x}_i) \phi_\theta^\top(\mathbf{x}_i)) U \right]$$

This motivates the introduction of the splitted loss. We now discuss the connections with probabilistic models and independence of latent factors.

3 Connections with the Evidence Lower Bound

In order to formulate an ELBO for our proposed model, two other random encoders are used:

$$q(\mathbf{z}|\mathbf{x}) = \mathcal{N}(\mathbf{z}|\phi_\theta(\mathbf{x}), \gamma^2 \mathbb{I}_\ell) \text{ and } q_U(\mathbf{z}|\mathbf{x}) = \mathcal{N}(\mathbf{z}|\mathbb{P}_U \phi_\theta(\mathbf{x}), \sigma^2 \mathbb{P}_U + \delta^2 \mathbb{P}_{U^\perp})$$

where ϕ_θ has zero mean on the data distribution. Here, σ^2 plays the role of a trade-off parameter, while the regularization parameter δ is introduced for technical reasons and is put to a numerically small value (for details, see Appendix A.3). Let the decoder be $p(\mathbf{x}|\mathbf{z}) = \mathcal{N}(\mathbf{x}|\psi(\mathbf{z}), \sigma_0^2 \mathbb{I})$ and the latent space distribution is parametrized by $p(\mathbf{z}) = \mathcal{N}(0, \Sigma)$ where Σ is a $\ell \times \ell$ covariance matrix that is determined at the last stage of the training. Contrary to VAEs where the latent space distribution is ‘a priori’ $\mathcal{N}(0, \mathbb{I})$, we treat here the covariance matrix Σ as a parameter of the optimization problem. The minimization problem (7) with stochastic AE loss is equivalent to the maximization of

$$\frac{1}{n} \sum_{i=1}^n \left\{ \underbrace{\mathbb{E}_{q_U(\mathbf{z}|\mathbf{x}_i)}[\log(p(\mathbf{x}_i|\mathbf{z}))]}_{\text{(I)}} - \underbrace{\text{KL}(q_U(\mathbf{z}|\mathbf{x}_i), q(\mathbf{z}|\mathbf{x}_i))}_{\text{(II)}} - \underbrace{\text{KL}(q_U(\mathbf{z}|\mathbf{x}_i), p(\mathbf{z}))}_{\text{(III)}} \right\}, \quad (9)$$

which is a lower bound to the ELBO, since the KL divergence in (II) is positive. We do not optimize here over the hyper-parameters γ, σ, σ_0 which take a fixed value. Up to additive constants, the terms (I) and (II) of (9) match the objective (7). The third term (III) in (9) is optimized after the training of the first two terms. It can be written as follows

$$\frac{1}{n} \sum_{i=1}^n \text{KL}(q_U(\mathbf{z}|\mathbf{x}_i), p(\mathbf{z})) = \frac{1}{2} \text{Tr}[\Sigma_0 \Sigma^{-1}] + \frac{1}{2} \log(\det \Sigma) + \text{constants}$$

with $\Sigma_0 = \mathbb{P}_U C_\theta \mathbb{P}_U + \sigma^2 \mathbb{P}_U + \delta^2 \mathbb{P}_{U^\perp}$. Hence, in that case, the optimal covariance matrix is diagonalized $\Sigma = U(\text{diag}(\boldsymbol{\lambda}) + \sigma^2 \mathbb{I}_m)U^\top + \delta^2 \mathbb{P}_{U^\perp}$, with $\boldsymbol{\lambda}$ denoting the principal values of the PCA. Let us briefly discuss the factorization of the encoder. Let $\mathbf{h}(\mathbf{x}) = U^\top \phi_\theta(\mathbf{x})$ and let the ‘effective’ latent variable be $\mathbf{z}^{(U)} = U^\top \mathbf{z} \in \mathbb{R}^m$. The pdf of $q_U(\mathbf{z}|\mathbf{x})$ is

$$f_{q_U(\mathbf{z}|\mathbf{x})}(\mathbf{z}) = \frac{e^{-\frac{\|U^\top \mathbf{z}\|_2^2}{2\delta^2}}}{(\sqrt{2\pi\delta^2})^{\ell-m}} \prod_{j=1}^m \frac{e^{-\frac{(\mathbf{z}_j^{(U)} - \mathbf{h}_j(\mathbf{x}))^2}{2\sigma^2}}}{\sqrt{2\pi\sigma^2}},$$

where the first factor is approximated by a Dirac delta if $\delta \rightarrow 0$. Hence, the factorized form of pdf of q_U indicates the independence of the latent variables $\mathbf{z}^{(U)}$. This independence has been argued to promote disentanglement. Namely, the term (II) in (9) is analogous to a ‘Total Correlation’ loss [4], although not formally equal.

4 Experiments

In this section we empirically evaluate St-RKM. In particular we investigate if the model can simultaneously achieve (i) accurate reconstructions on training data (ii) good random generations and (iii) good disentanglement performance. We use datasets commonly used to evaluate generative models such as MNIST [13], Fashion-MNIST [29] (fMNIST) and SVHN [20]. Furthermore, in order to evaluate disentanglement, we use datasets with known ground-truth generating factors such as Dsprites [18], 3Dshapes [2] and Cars3D [23].

Algorithm We use an alternating-minimization scheme (see Algorithm 1 in Appendix). First, the ADAM optimizer with learning rate 2×10^{-4} is used to update the encoder-decoder parameters and then, the Cayley ADAM optimizer with learning rate 10^{-4} is used to update the U . Finally, at the end of the training, we recompute U from the SVD of the covariance matrix as a final correction-step of the Kernel PCA term in our objective. Since the $\ell \times \ell$ covariance matrix is typically small, this decomposition is fast. In practice, this only marginally increases the computation cost as can be seen from training times in Table 2.

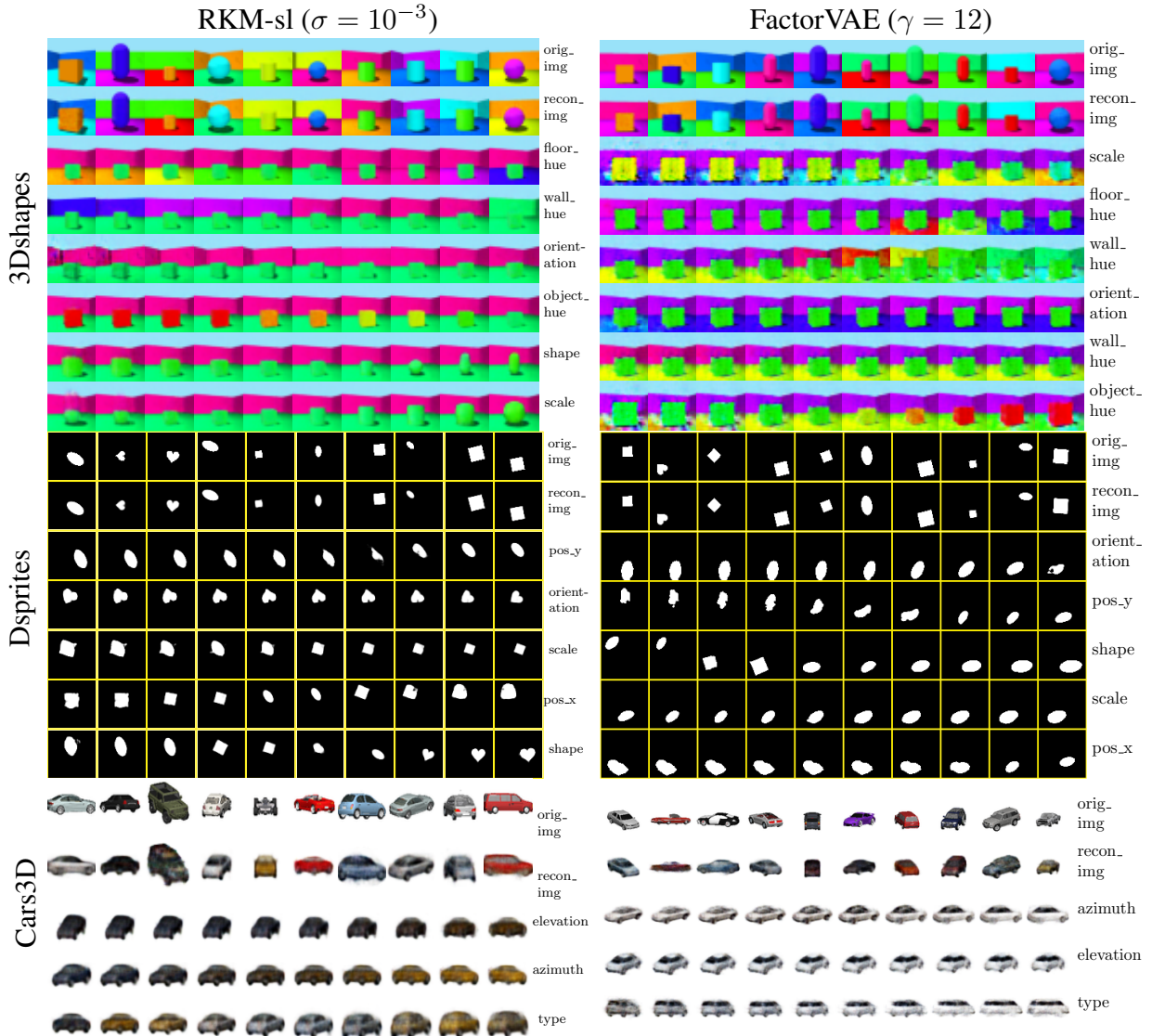


Figure 2: Traversals along principal components. First-two rows show the ground-truth and reconstructed images and each subsequent row show the generated images by traversing along a principal component in the latent space. The last column in each images shows the dominant factor of variation.

Experimental setup: We consider four baselines for comparison: (i) VAE, (ii) β -VAE, (iii) FactorVAE and (iv) Info-GAN. To be consistent in evaluation, we keep the same encoder (discriminator) and decoder (generator) architecture; and same latent dimension across the models. In the case of Info-GAN, batch-normalization is added for training stability. For the determination of the hyperparameters of other methods, we start from values in the range of the parameters suggested in the authors’ reference implementation. After trying various values we noticed that $\beta = 3$ and $\gamma = 12$ seem to work good across all datasets we considered for the β -VAE and FactorVAE respectively. Furthermore, in all experiments on St-RKM, we keep reconstruction weight $\lambda = 1$. All models are trained on the entire datasets. Further technical details are given in Appendix B. Note that for the same encoder-decoder network, St-RKM model has the least number of parameters compared to any VAE variants and Info-GAN (see Table 2). The difference becomes apparent in the bottleneck part, where the VAEs use additional networks to parameterize

Table 2: Training time [number of training parameters] comparisons (in minutes) on full MNIST dataset over 10 runs.

St-RKM	β -VAE	FactorVAE	Info-GAN
[4164519]	[4165589]	[8182591]	[4713478]
21.93 (± 1.3)	19.83 (± 0.8)	33.31 (± 2.7)	45.96 (± 1.6)

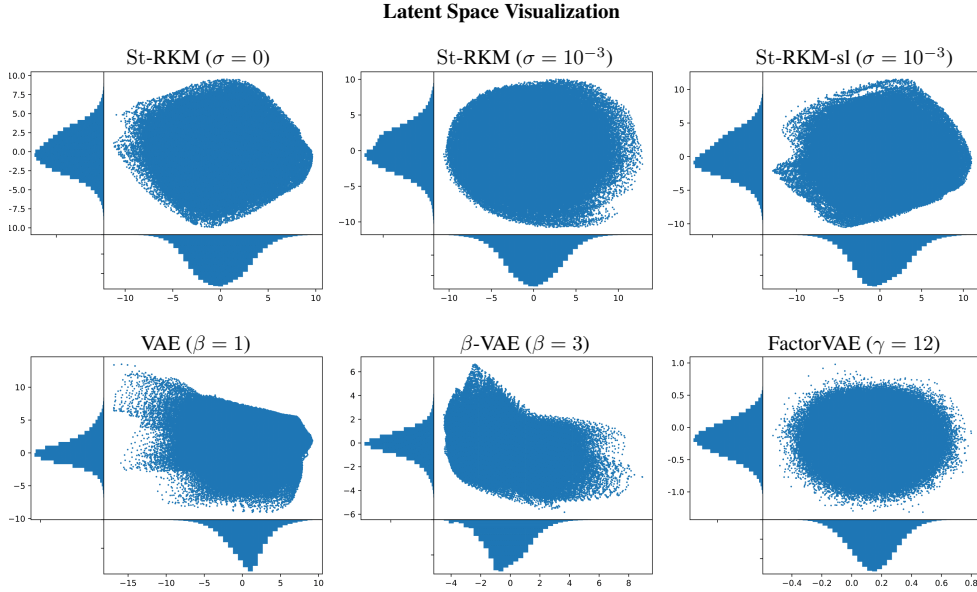


Figure 3: Scatter plots of latent variables with histograms. The models were trained on full Dsprites dataset (737280 points). In the case of St-RKMs, the joint distributions are always centered around zero and are elliptically distributed.

the mean and variance of the normal latent distribution. Similarly in Info-GAN, an auxiliary network is used in the variational information maximization setting.

To quantitatively assess the quality of generated samples we use Fréchet Inception Distance [8] (FID) scores and the Sliced Wasserstein Distance (SWD) [10]. We report the results for FID in Table 1. Notice the improvement in SWD scores for RKM variants for Dsprites dataset (see Table 6). Randomly generated samples are shown in Figure 6. To generate samples from deterministic St-RKM ($\sigma = 0$), we sample from a fitted normal distribution on the latent embeddings of the dataset. This is motivated by the first-term in objective (4), which puts an implicit prior on the latent distribution. Empirically, this is confirmed by Figure 3, which shows the scatter plot of the first-two components of latent variables. For St-RKMs, those latent variables correspond to the principal components with the largest eigenvalues. In the case of VAEs, it is also meaningful to select the first-two latent variables since there is an isotropic Gaussian-prior over latent variables. As can be seen, St-RKM variants perform better on most datasets and within them, the stochastic variants with $\sigma = 10^{-3}$ performs the best. This can be attributed to better generalization of the decoder network due to the addition of noise-term on latent-variables (see Lemma 1). The SWD confirms this trend, where the RKM variants show a lower SWD on average. The training times for St-RKM models are slightly higher compared to standard VAE but outperforms FactorVAE and Info-GAN due to significantly less number of training parameters.

To quantitatively evaluate the disentanglement performance, various metrics have been proposed. A comprehensive review by Locatello et al. [16] shows that the various disentanglement metrics are correlated albeit with different degree of correlation across datasets. In this paper, we use three measures given in Eastwood’s framework [6]: *disentanglement*: the degree to which a representation factorises the underlying factors of variation, with each variable capturing at most one generative factor; *completeness*: the degree to which each underlying factor is captured by a single code variable; and *informativeness*: the amount of information that a representation captures about the underlying factors of variation. As a sanity check, we also evaluate β -VAE and FactorVAE scores and report the results in Figure 5 in Appendix. Table 3 shows that St-RKM variants have better disentanglement and completeness scores while barely sacrificing the reconstruction errors (see Figure 4). However, informativeness scores are higher for St-RKM when using a lasso-regressor in contrast to mixed scores with Random forest regressor. This can be seen more clearly in Figure 2 which shows the generated images by traversing along the principal components in the latent space. In 3Dshapes dataset, St-RKM model captures floor-hue, wall-hue and orientation perfectly but has a slight entanglement in capturing other factors. This gets worse in β -VAE which has entanglement in all dimensions except the floor-hue along with noise in some generated images. This may be due to the inherent trade-off in the model which is also apparent from its low FID scores. Similar trends can be observed in Dsprites and Cars3D dataset. Low scores of Info-GAN are not surprising given that the model is very sensitive to architecture choices compared to VAE and its variants, which are more robust to such choices [11]. This can be a disadvantage for Info-GAN in situations where architecture search is important.

Table 3: Eastwood framework’s [6] disentanglement metric with Lasso and Random Forest regressor. For disentanglement and completeness higher score is better, for informativeness, lower is better. Average model scores. ‘Info.’ indicates (average) root-mean-square error in predicting z . Best scores are in bold.

Dataset	Model	Lasso			Random Forest		
		Dise.	Comp.	Info.	Dise.	Comp.	Info.
Dsprites	St-RKM ($\sigma = 0$)	0.41 (± 0.02)	0.45 (± 0.01)	1.05 (± 0.03)	0.27 (± 0.01)	0.62 (± 0.01)	0.97 (± 0.03)
	St-RKM ($\sigma = 10^{-3}$)	0.45 (± 0.01)	0.47 (± 0.02)	1.05 (± 0.01)	0.28 (± 0.01)	0.63 (± 0.02)	1.02 (± 0.01)
	St-RKM-sl ($\sigma = 10^{-3}$)	0.37 (± 0.03)	0.32 (± 0.01)	1.07 (± 0.02)	0.35 (± 0.02)	0.58 (± 0.01)	0.96 (± 0.02)
	VAE ($\beta = 1$)	0.26 (± 0.06)	0.22 (± 0.00)	0.97 (± 0.01)	0.24 (± 0.03)	0.55 (± 0.04)	1.00 (± 0.01)
	β -VAE ($\beta = 3$)	0.36 (± 0.02)	0.31 (± 0.02)	0.96 (± 0.21)	0.33 (± 0.01)	0.53 (± 0.04)	0.99 (± 0.11)
	FactorVAE ($\gamma = 12$)	0.40 (± 0.01)	0.34 (± 0.01)	0.98 (± 0.01)	0.34 (± 0.02)	0.58 (± 0.01)	1.05 (± 0.01)
	Info-GAN	0.31 (± 0.21)	0.27 (± 0.03)	0.95 (± 0.02)	0.31 (± 0.01)	0.47 (± 0.20)	1.00 (± 0.02)
3Dshapes	St-RKM ($\sigma = 0$)	0.76 (± 0.02)	0.71 (± 0.02)	1.06 (± 0.03)	0.55 (± 0.03)	0.69 (± 0.02)	0.51 (± 0.21)
	St-RKM ($\sigma = 10^{-3}$)	0.74 (± 0.02)	0.66 (± 0.01)	1.24 (± 0.02)	0.61 (± 0.01)	0.67 (± 0.01)	0.86 (± 0.10)
	St-RKM-sl ($\sigma = 10^{-3}$)	0.72 (± 0.01)	0.65 (± 0.01)	1.03 (± 0.02)	0.63 (± 0.02)	0.66 (± 0.02)	0.95 (± 0.01)
	VAE ($\beta = 1$)	0.44 (± 0.21)	0.33 (± 0.22)	1.26 (± 0.20)	0.33 (± 0.20)	0.36 (± 0.21)	0.94 (± 0.01)
	β -VAE ($\beta = 3$)	0.55 (± 0.01)	0.54 (± 0.01)	1.07 (± 0.01)	0.56 (± 0.01)	0.57 (± 0.03)	0.54 (± 0.22)
	FactorVAE ($\gamma = 12$)	0.62 (± 0.01)	0.41 (± 0.03)	1.05 (± 0.01)	0.57 (± 0.02)	0.58 (± 0.01)	0.93 (± 0.20)
	Info-GAN	0.41 (± 0.22)	0.39 (± 0.01)	1.17 (± 0.02)	0.53 (± 0.01)	0.51 (± 0.10)	0.61 (± 0.12)
Cars3D	St-RKM ($\sigma = 0$)	0.45 (± 0.01)	0.27 (± 0.13)	1.33 (± 0.08)	0.49 (± 0.01)	0.38 (± 0.01)	1.16 (± 0.03)
	St-RKM ($\sigma = 10^{-3}$)	0.42 (± 0.09)	0.40 (± 0.02)	1.34 (± 0.03)	0.54 (± 0.01)	0.32 (± 0.02)	1.20 (± 0.11)
	St-RKM-sl ($\sigma = 10^{-3}$)	0.65 (± 0.02)	0.48 (± 0.01)	1.30 (± 0.05)	0.55 (± 0.02)	0.33 (± 0.02)	1.20 (± 0.03)
	VAE ($\beta = 1$)	0.47 (± 0.01)	0.18 (± 0.04)	1.34 (± 0.02)	0.23 (± 0.21)	0.35 (± 0.01)	1.21 (± 0.02)
	β -VAE ($\beta = 3$)	0.51 (± 0.06)	0.27 (± 0.08)	1.35 (± 0.01)	0.47 (± 0.07)	0.37 (± 0.02)	1.19 (± 0.07)
	FactorVAE ($\gamma = 12$)	0.54 (± 0.02)	0.38 (± 0.23)	1.33 (± 0.02)	0.44 (± 0.01)	0.33 (± 0.01)	1.24 (± 0.01)
	Info-GAN	0.56 (± 0.01)	0.23 (± 0.13)	1.29 (± 0.04)	0.27 (± 0.22)	0.32 (± 0.05)	1.41 (± 0.21)

5 Conclusion

In this paper, a new representation learning method, St-RKM, was proposed and compared to recent variants of variational auto-encoders. As discussed, the explicit optimization on the Stiefel manifold promotes an improved disentanglement, with a marginal increase in computational time. An additional advantage of St-RKM is that the number of parameters of the model is comparable to a vanilla VAE. Our numerical study shows in several cases an improvement of the generation and disentanglement quality over several datasets. Among the possible regularizers on the hidden features, the models associated to the squared Euclidean norm were analysed in detail, while a deeper study of other regularizers is a prospect for further research, in particular for the case of spherical units mentioned in the introduction.

Acknowledgment

EU: The research leading to these results has received funding from the European Research Council under the European Union’s Horizon 2020 research and innovation program / ERC Advanced Grant E-DUALITY (787960). This paper reflects only the authors’ views and the Union is not liable for any use that may be made of the contained information. Research Council KUL: Optimization frameworks for deep kernel machines C14/18/068 Flemish Government: FWO: projects: GOA4917N (Deep Restricted Kernel Machines: Methods and Foundations), PhD/Postdoc grant Impulsfonds AI: VR 2019 2203 DOC.0318/1QUATER Kenniscentrum Data en Maatschappij Ford KU Leuven Research Alliance Project KUL0076 (Stability analysis and performance improvement of deep reinforcement learning algorithms). The computational resources and services used in this work were provided by the VSC (Flemish Supercomputer Center), funded by the Research Foundation - Flanders (FWO) and the Flemish Government – department EWI.

References

- [1] Yoshua Bengio, Aaron Courville, and Pascal Vincent. Representation learning: A review and new perspectives. *IEEE Transactions on Pattern Analysis and Machine Intelligence*, 35(8):1798–1828, 2013.
- [2] Chris Burgess and Hyunjik Kim. 3d shapes dataset. <https://github.com/deepmind/3dshapes-dataset/>, 2018.
- [3] Christopher P Burgess, Irina Higgins, Arka Pal, Loic Matthey, Nick Watters, Guillaume Desjardins, and Alexander Lerchner. Understanding disentangling in β -VAE. *Advances in Neural Information Processing Systems*, 2017.
- [4] Ricky T. Q. Chen, Xuechen Li, Roger B Grosse, and David K Duvenaud. Isolating sources of disentanglement in variational autoencoders. In *Advances in Neural Information Processing Systems 31*, pages 2610–2620, 2018.
- [5] Vincent Dumoulin and Francesco Visin. A guide to convolution arithmetic for deep learning. *arXiv preprint arXiv:1603.07285*, 2016.
- [6] Cian Eastwood and Christopher K. I. Williams. A framework for the quantitative evaluation of disentangled representations. In *proceedings of the International Conference on Learning Representations (ICLR)*, 2018.
- [7] Partha Ghosh, Mehdi SM Sajjadi, Antonio Vergari, Michael Black, and Bernhard Schölkopf. From variational to deterministic autoencoders. In *proceedings of the International Conference on Learning Representations (ICLR)*, 2020.
- [8] Martin Heusel, Hubert Ramsauer, Thomas Unterthiner, Bernhard Nessler, and Sepp Hochreiter. GANs trained by a two time-scale update rule converge to a local Nash equilibrium. In *Advances in Neural Information Processing Systems*, pages 6629–6640, 2017.
- [9] Irina Higgins, Loic Matthey, Arka Pal, Christopher Burgess, Xavier Glorot, Matthew Botvinick, Shakir Mohamed, and Alexander Lerchner. Beta-VAE: Learning basic visual concepts with a constrained variational framework. In *proceedings of the International Conference on Learning Representations (ICLR)*, volume 2, page 6, 2017.
- [10] Tero Karras, Timo Aila, Samuli Laine, and Jaakko Lehtinen. Progressive growing of GANs for improved quality, stability, and variation. In *proceedings of the International Conference on Learning Representations (ICLR)*, 2017.
- [11] Hyunjik Kim and Andriy Mnih. Disentangling by factorising. In *proceedings of the Thirty-fifth International Conference on Machine Learning (ICML)*, volume 80, pages 2649–2658, 2018.
- [12] Diederik P. Kingma and Max Welling. Auto-Encoding Variational Bayes. In *proceedings of the International Conference on Learning Representations (ICLR)*, 2014.
- [13] Yann LeCun and Corinna Cortes. MNIST handwritten digit database. <http://yann.lecun.com/exdb/mnist/>, 2010.
- [14] Yann LeCun, Fu Jie Huang, and Leon Bottou. Learning methods for generic object recognition with invariance to pose and lighting. In *Computer Vision and Pattern Recognition (CVPR)*, volume 2, 2004.
- [15] Jun Li, Fuxin Li, and Sinisa Todorovic. Efficient riemannian optimization on the stiefel manifold via the cayley transform. In *proceedings of the International Conference on Learning Representations (ICLR)*, 2020.
- [16] Francesco Locatello, Stefan Bauer, Mario Lučić, Gunnar Rätsch, Sylvain Gelly, Bernhard Schölkopf, and Olivier Frederic Bachem. Challenging common assumptions in the unsupervised learning of disentangled representations. In *proceedings of the Thirty-sixth International Conference on Machine Learning (ICML)*, 2019.
- [17] Francesco Locatello, Michael Tschannen, Stefan Bauer, Gunnar Rätsch, Bernhard Schölkopf, and Olivier Bachem. Disentangling factors of variations using few labels. In *proceedings of the International Conference on Learning Representations (ICLR)*, 2020.
- [18] Loic Matthey, Irina Higgins, Demis Hassabis, and Alexander Lerchner. dsprites: Disentanglement testing sprites dataset. <https://github.com/deepmind/dsprites-dataset/>, 2017.
- [19] Yurii Nesterov. *Introductory Lectures on Convex Optimization: A Basic Course*. Springer Publishing Company, Incorporated, 1st edition, 2014.
- [20] Yuval Netzer, Tao Wang, Adam Coates, Alessandro Bissacco, Bo Wu, and Andrew Y Ng. Reading digits in natural images with unsupervised feature learning. In *NIPS Workshop on Deep Learning and Unsupervised Feature Learning*, 2011.
- [21] Arun Pandey, Joachim Schreurs, and Johan A. K. Suykens. Generative Restricted Kernel Machines. *arXiv preprint arXiv:1906.08144*, 2019.
- [22] Arun Pandey, Joachim Schreurs, and Johan A. K. Suykens. Robust Generative Restricted Kernel Machines using weighted conjugate feature duality. *arXiv preprint arXiv:2002.01180*, 2020.
- [23] Scott Reed, Yi Zhang, Yuting Zhang, and Honglak Lee. Deep visual analogy-making. In *Advances in Neural Information Processing Systems*, 2015.
- [24] Danilo Jimenez Rezende and Shakir Mohamed. Variational Inference with Normalizing Flows. *proceedings of the Thirty-second International Conference on Machine Learning (ICML)*, 2015.
- [25] M. Rolínek, D. Zietlow, and G. Martius. Variational Autoencoders pursue PCA directions (by accident). In *2019 IEEE/CVF Conference on Computer Vision and Pattern Recognition (CVPR)*, pages 12398–12407, 2019.

- [26] Ruslan Salakhutdinov and Geoffrey Hinton. Deep Boltzmann Machines. In *proceedings of the Twelfth International Conference on Artificial Intelligence and Statistics*, volume 5 of JMLR, 2009.
- [27] Bernhard Scholkopf and Alexander J. Smola. *Learning with Kernels: Support Vector Machines, Regularization, Optimization, and Beyond*. MIT Press, Cambridge, MA, USA, 2001.
- [28] Johan A. K. Suykens. Deep Restricted Kernel Machines using conjugate feature duality. *Neural Computation*, 29(8):2123–2163, August 2017.
- [29] Han Xiao, Kashif Rasul, and Roland Vollgraf. Fashion-MNIST: A novel image dataset for benchmarking machine learning algorithms. *ArXiv preprint arXiv:1708.07747*, 2017.

A Additional details

A.1 Units on the sphere

In the case of spherical units, one obtains the following objective

$$\min_{U \in \text{St}(\ell, m)} \min_{\theta, \xi} \frac{1}{n} \sum_{i=1}^n \{ \|\phi_{\theta}(\mathbf{x}_i)\|_2 - \|\mathbb{P}_U \phi_{\theta}(\mathbf{x}_i)\|_2 + \gamma L_{\xi, U}(\mathbf{x}_i, \phi_{\theta}(\mathbf{x}_i)) \}. \quad (10)$$

where we used the expression of the Fenchel conjugate of $f(\mathbf{h}) = \chi_{\mathbb{S}^{m-1}}(\mathbf{h})$. Indeed, consider the optimization problem

$$\min_{\mathbf{h}_i \in \mathbb{S}^{m-1}} -\phi(\mathbf{x}_i)^{\top} \mathbf{U} \mathbf{h}_i, \quad (11)$$

where the penalty has been replaced by a constraint $\|\mathbf{h}_i\|_2 = 1$. Clearly, by looking at (11), the solution is a projection on the sphere $\mathbf{h}_i^* = U^{\top} \phi(\mathbf{x}_i) / \|U^{\top} \phi(\mathbf{x}_i)\|_2$. Then, we have

$$\min_{U \in \text{St}(\ell, m)} \min_{\mathbf{h}_i \in \mathbb{S}^{m-1}} \sum_{i=1}^n -\phi(\mathbf{x}_i)^{\top} \mathbf{U} \mathbf{h}_i = \min_{U \in \text{St}(\ell, m)} - \sum_{i=1}^n \|U^{\top} \phi(\mathbf{x}_i)\|_2, \quad (12)$$

Other PCA with sum of errors rather than sum of squared error.

A.2 Proof of Lemma 1

We first quote a result that is used in the context of optimization ([19], Lemma 1.2.4). Let f a function with L -Lipschitz continuous Hessian. Then, it holds

$$\underbrace{\left| f(\mathbf{y}_1) - f(\mathbf{y}) - \nabla f(\mathbf{y})^{\top} (\mathbf{y}_1 - \mathbf{y}) - \frac{1}{2} (\mathbf{y}_1 - \mathbf{y})^{\top} \text{Hess}_{\mathbf{y}}[f] (\mathbf{y}_1 - \mathbf{y}) \right|}_{r(\mathbf{y}_1 - \mathbf{y})} \leq \frac{L}{6} \|\mathbf{y}_1 - \mathbf{y}\|_2^3. \quad (13)$$

Then, we calculate the power series expansion of $f(\mathbf{y}) = [\mathbf{x} - \psi(\mathbf{y})]_a^2$ and take the expectation with respect to $\epsilon \sim \mathcal{N}(0, \mathbb{I})$. Firstly, we have

$$\nabla f(\mathbf{y}) = -2[\mathbf{x} - \psi(\mathbf{y})]_a \nabla \psi_a(\mathbf{y})$$

and

$$\text{Hess}_{\mathbf{y}}[f] = 2\nabla \psi_a(\mathbf{y}) \nabla \psi_a(\mathbf{y})^{\top} - 2[\mathbf{x} - \psi(\mathbf{y})]_a \text{Hess}_{\mathbf{y}}[\psi_a].$$

Then, we use (13) with $\mathbf{y}_1 - \mathbf{y} = \sigma U \epsilon$. By taking the expectation over ϵ , notice that the order 1 term in σ vanishes since $\mathbb{E}_{\epsilon}[\epsilon] = 0$. We find

$$\begin{aligned} \mathbb{E}_{\epsilon} [\mathbf{x} - \psi(\mathbf{y} + \sigma U \epsilon)]_a^2 &= [\mathbf{x} - \psi(\mathbf{y})]_a^2 + \sigma^2 \text{Tr} (U^{\top} \nabla \psi_a(\mathbf{y}) \nabla \psi_a(\mathbf{y})^{\top} U) \\ &\quad - \sigma^2 [\mathbf{x} - \psi(\mathbf{y})]_a \text{Tr} (U^{\top} \text{Hess}_{\mathbf{y}}[\psi_a] U) + \mathbb{E}_{\epsilon} r(\sigma U \epsilon), \end{aligned}$$

where we used that $\mathbb{E}_{\epsilon}[\epsilon^{\top} M \epsilon] = \text{Tr}[M]$ for any symmetric matrix M since $\mathbb{E}_{\epsilon}[\epsilon_i \epsilon_j] = \delta_{ij}$. Next, denote $R_a(\sigma) = \mathbb{E}_{\epsilon} r(\sigma U \epsilon)$ we can use the Jensen inequality and subsequently (13)

$$|R_a(\sigma)| = |\mathbb{E}_{\epsilon} r(\sigma U \epsilon)| \leq \mathbb{E}_{\epsilon} |r(\sigma U \epsilon)| \leq \frac{L}{6} \mathbb{E}_{\epsilon} \|\sigma U \epsilon\|_2^3.$$

Next, we notice that $\|\sigma U \epsilon\|_2 = \sigma (\epsilon^{\top} U^{\top} U \epsilon)^{1/2} = \sigma \|\epsilon\|_2$. It is useful to notice that $\|\epsilon\|_2$ is distributed according to a chi distribution. By using this remark, we find

$$|R_a(\sigma)| \leq \sigma^3 \frac{L}{6} \mathbb{E}_{\epsilon} \|\epsilon\|_2^3 = \sigma^3 \frac{L}{6} \frac{\sqrt{2}(m+1)\Gamma((m+1)/2)}{\Gamma(m/2)},$$

where the last equality uses the expression for the third moment of the chi distribution and where the Gamma function Γ is the extension of the factorial to the complex numbers.

A.3 Details on Evidence Lower Bound for St-RKM model

We discuss here the technical details associated to the ELBO given in section 3. The first term in (9) is

$$\mathbb{E}_{q_U(\mathbf{z}|\mathbf{x}_i)}[\log(p(\mathbf{x}_i|\mathbf{z}))] = \frac{1}{2\sigma_0^2} \mathbb{E}_{\epsilon \sim \mathcal{N}(0, \mathbb{I})} \|\mathbf{x}_i - \psi_\xi(\mathbb{P}_U \phi_\theta(\mathbf{x}_i) + \sigma \mathbb{P}_U \epsilon + \delta \mathbb{P}_{U^\perp} \epsilon)\|_2^2 - \frac{d}{2} \log(2\pi\sigma_0^2).$$

Clearly, the above expectation can be written as follows

$$\mathbb{E}_{\epsilon \sim \mathcal{N}(0, \mathbb{I}_m)} \mathbb{E}_{\epsilon_\perp \sim \mathcal{N}(0, \mathbb{I}_{\ell-m})} \|\mathbf{x}_i - \psi_\xi(\mathbb{P}_U \phi_\theta(\mathbf{x}_i) + \sigma U \epsilon + \delta U_\perp \epsilon_\perp)\|_2^2.$$

Hence, we fix $\sigma_0^2 = 1/2$ and take $\delta > 0$ to a numerically small value. For the other terms of (9), we use the formula giving the KL divergence between multivariate normals. Let \mathcal{N}_0 and \mathcal{N}_1 be ℓ -variate normal distributions with mean μ_0, μ_1 and covariance Σ_0, Σ_1 respectively. Then,

$$\text{KL}(\mathcal{N}_0, \mathcal{N}_1) = \frac{1}{2} \left\{ \text{Tr}(\Sigma_1^{-1} \Sigma_0) + (\mu_1 - \mu_0)^\top \Sigma_1^{-1} (\mu_1 - \mu_0) - \ell + \log \left(\frac{\det \Sigma_1}{\det \Sigma_0} \right) \right\}$$

By using this identity, we find the second term of (9):

$$\begin{aligned} \text{KL}[q_U(\mathbf{z}|\mathbf{x}_i), q(\mathbf{z}|\mathbf{x}_i)] &= \frac{1}{2} \left\{ \frac{m\sigma^2 + (\ell - m)\delta^2}{\gamma^2} + \frac{1}{\gamma^2} \|\phi_\theta(\mathbf{x}_i) - \mathbb{P}_U \phi_\theta(\mathbf{x}_i)\|_2^2 \right. \\ &\quad \left. - \ell + \log \left(\frac{\gamma^{2\ell}}{\sigma^{2k} \delta^{2(\ell-m)}} \right) \right\}. \end{aligned}$$

For the third term in (9), we find

$$\begin{aligned} \text{KL}[q_U(\mathbf{z}|\mathbf{x}_i), p(\mathbf{z})] &= \frac{1}{2} \left\{ \text{Tr}((\sigma^2 \mathbb{P}_U + \delta^2 \mathbb{P}_{U^\perp}) \Sigma^{-1}) + (\mathbb{P}_U \phi_\theta(\mathbf{x}_i))^\top \Sigma^{-1} (\mathbb{P}_U \phi_\theta(\mathbf{x}_i)) \right. \\ &\quad \left. + \log \det(\Sigma) - \ell - \log(\sigma^{2m} \delta^{2(\ell-m)}) \right\}. \end{aligned}$$

By averaging over $i = 1, \dots, n$, we obtain

$$\begin{aligned} \frac{1}{n} \sum_{i=1}^n \text{KL}[q_U(\mathbf{z}|\mathbf{x}_i), p(\mathbf{z})] &= \frac{1}{2} \left\{ \text{Tr}((\sigma^2 \mathbb{P}_U + \delta^2 \mathbb{P}_{U^\perp}) \Sigma^{-1}) + \text{Tr}(\mathbb{P}_U C_\theta \mathbb{P}_U \Sigma^{-1}) \right. \\ &\quad \left. + \log \det(\Sigma) - \ell - \log(\sigma^{2m} \delta^{2(\ell-m)}) \right\}, \end{aligned}$$

where we used the cyclic property of the trace and $C_\theta = \frac{1}{n} \sum_{i=1}^n \phi_\theta(\mathbf{x}_i) \phi_\theta(\mathbf{x}_i)^\top$. This proves the analogous expression in section 3. Finally, the estimation of the optimal Σ can be done in parallel to the Maximum Likelihood Estimation of the covariance matrix of a multivariate normal.

B Datasets, Hyperparameters and Algorithm

See Table 4 and 5 for details on model architectures, datasets and hyperparameters used in this paper. All models were trained on full-datasets and for maximum 1000 epochs. Further all datasets are scaled between [0-1] and are resized to 28×28 dimensions except Dsprites and Cars3D. The PyTorch library in Python was used as the programming language on 8GB NVIDIA QUADRO P4000 GPU. See Algorithm 1 for training the St-RKM model. In the case of FactorVAE, the discriminator architecture is same as proposed in the original paper [11].

Table 4: Datasets and hyperparameters used for the experiments. N is the number of training samples, d the input dimension (resized images), m the subspace dimension and M the minibatch size.

Dataset	N	d	m	M
MNIST	60000	28×28	10	256
fMNIST	60000	28×28	10	256
SVHN	73257	$32 \times 32 \times 3$	10	256
Dsprites	737280	64×64	5	256
3Dshapes	480000	$64 \times 64 \times 3$	6	256
Cars3D	17664	$64 \times 64 \times 3$	3	256

C Further Empirical Results

Table 5: Model architectures. All convolutions and transposed-convolutions are with stride 2 and padding 1. Unless stated otherwise, layers have Parametric-RELU ($\alpha = 0.2$) activation functions, except output layers of the pre-image maps which have sigmoid activation functions (since input data is normalized $[0, 1]$). Adam and CayleyAdam optimizers have learning rates 2×10^{-4} and 10^{-4} respectively. Pre-image map/decoder network is always taken as transposed of feature-map/encoder network. $c = 48$ for Cars3D; and $c = 64$ for all others. Further, $\hat{k} = 3$ and stride 1 for MNIST, fMNIST, SVHN and 3Dshapes; and $\hat{k} = 4$ for others. SVHN and 3Dshapes are resized to 28×28 input dimensions.

Dataset	Architecture
MNIST/fMNIST/ /SVHN/3Dshapes/ Dsprites/Cars3D	$\phi_{\theta}(\cdot) = \begin{cases} Conv [c] \times 4 \times 4; \\ Conv [c \times 2] \times 4 \times 4; \\ Conv [c \times 4] \times \hat{k} \times \hat{k}; \\ FC 256; \\ FC 50 (Linear) \end{cases} \quad \psi_{\zeta}(\cdot) = \begin{cases} FC 256; \\ FC [c \times 4] \times \hat{k} \times \hat{k}; \\ Conv [c \times 2] \times 4 \times 4; \\ Conv [c] \times 4 \times 4; \\ Conv [c] (Sigmoid) \end{cases}$

Algorithm 1 Manifold optimization of St-RKM

Input: $\{x_i\}_{i=1}^n, \phi_{\theta}, \psi_{\zeta}, \mathcal{J} := \text{Eq. 7}$

Output: Learned θ, ζ, U

```

1: procedure TRAIN
2:   while not converged do
3:      $\{x\} \leftarrow \{\text{Get mini-batch}\}$ 
4:     Get embeddings  $\phi_{\theta}(x) \leftarrow x$ 
5:     Compute centered  $C_{\theta}$ 
6:     Update  $\{\theta_e, \psi_g\} \leftarrow \text{ADAM}(\mathcal{J})$ 
7:     Update  $\{U\} \leftarrow \text{Cayley\_ADAM}(\mathcal{J})$ 
8:   end while
9:   Do steps 4-5 over whole dataset
10:   $U \leftarrow \text{SVD}(C_{\theta})$ 
11: end procedure

```

Table 6: Sliced Wasserstein Distance (SWD) to evaluate the quality of randomly generated 8000 samples over 10 iterations (smaller is better). The multi-scale statistical similarity between distributions of local image patches drawn from Laplacian pyramid are evaluated using the SWD. A small Wasserstein distance indicates that the distribution of the patches is similar, thus real and fake images appear similar in both appearance and variation at this spatial resolution. We always show the average SWD to evaluate performance. Scores are multiplied by 10^2 for better readability.

Models	MNIST	fMNIST	SVHN	3Dshapes	DSprites	Cars3D
St-RKM ($\sigma = 0$)	4.80 (± 0.13)	4.71 (± 0.14)	4.36 (± 0.32)	2.52 (± 0.18)	4.54 (± 0.64)	3.69 (± 1.4)
St-RKM ($\sigma = 10^{-3}$)	4.77 (± 0.12)	6.46 (± 0.17)	3.26 (± 0.16)	1.04 (± 0.14)	3.72 (± 0.58)	3.62 (± 1.29)
St-RKM-sl ($\sigma = 10^{-3}$)	3.11 (± 0.10)	5.17 (± 0.10)	4.16 (± 0.23)	1.20 (± 0.19)	3.13 (± 0.54)	4.02 (± 1.40)
VAE ($\beta = 1$)	4.85 (± 0.48)	5.60 (± 0.09)	4.50 (± 0.34)	2.06 (± 0.13)	5.04 (± 0.92)	4.01 (± 1.90)
β -VAE ($\beta = 3$)	3.75 (± 0.08)	7.16 (± 0.28)	4.71 (± 0.27)	3.25 (± 0.27)	4.85 (± 0.68)	4.83 (± 0.21)
FactorVAE ($\gamma = 12$)	3.52 (± 0.27)	5.12 (± 0.01)	3.46 (± 0.64)	1.32 (± 0.01)	3.24 (± 0.02)	3.47 (± 0.07)
InfoGAN	4.08 (± 0.27)	5.21 (± 1.33)	4.84 (± 0.72)	2.33 (± 0.36)	5.17 (± 0.31)	4.92 (± 0.33)

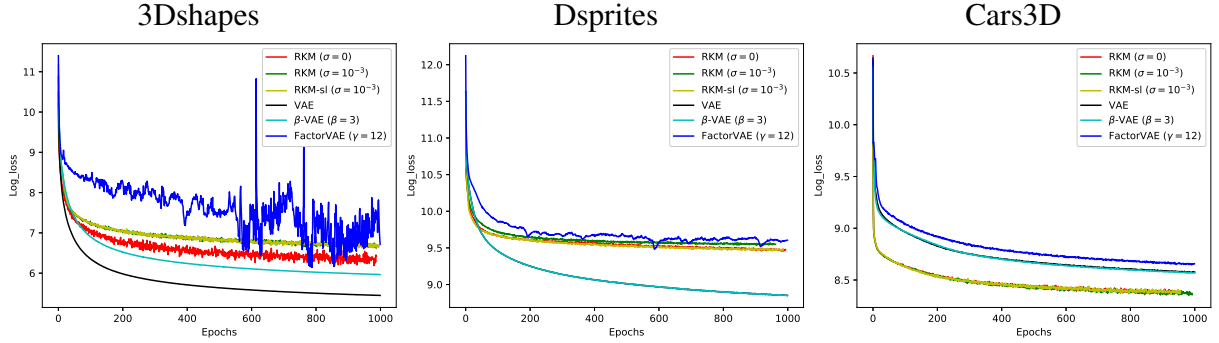


Figure 4: Reconstruction errors (log-scale) of various models during the training process over 1000 epochs.

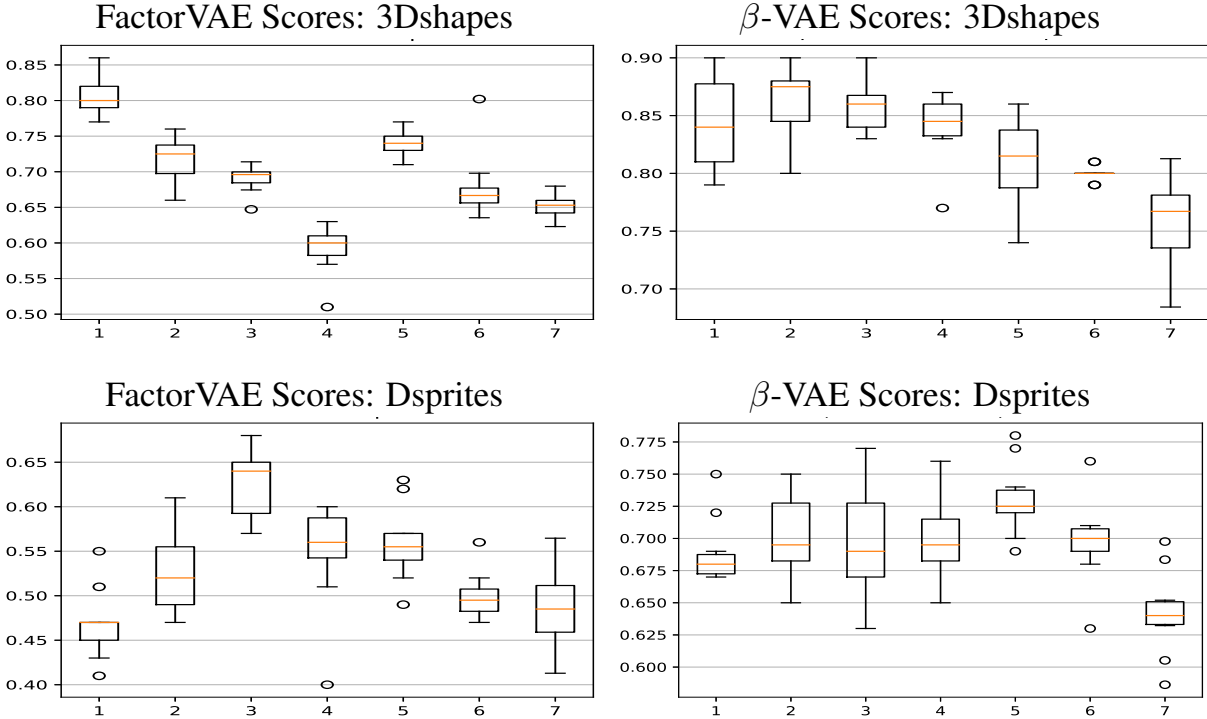


Figure 5: Box-plot of β -VAE [9] and FactorVAE [11] disentanglement scores (higher is better) over 10 iterations. x -axis represents the indices of models as follows: [1=St-RKM], [2=St-RKM ($\sigma = 10^{-3}$)], [3=St-RKM-sl ($\sigma = 10^{-3}$)], [4=VAE], [5= β -VAE], [6=FactorVAE], [7=Info-GAN]. In each subplot, highest average scores are obtained by St-RKM variants except in the case of β -VAE score on Dsprites dataset.

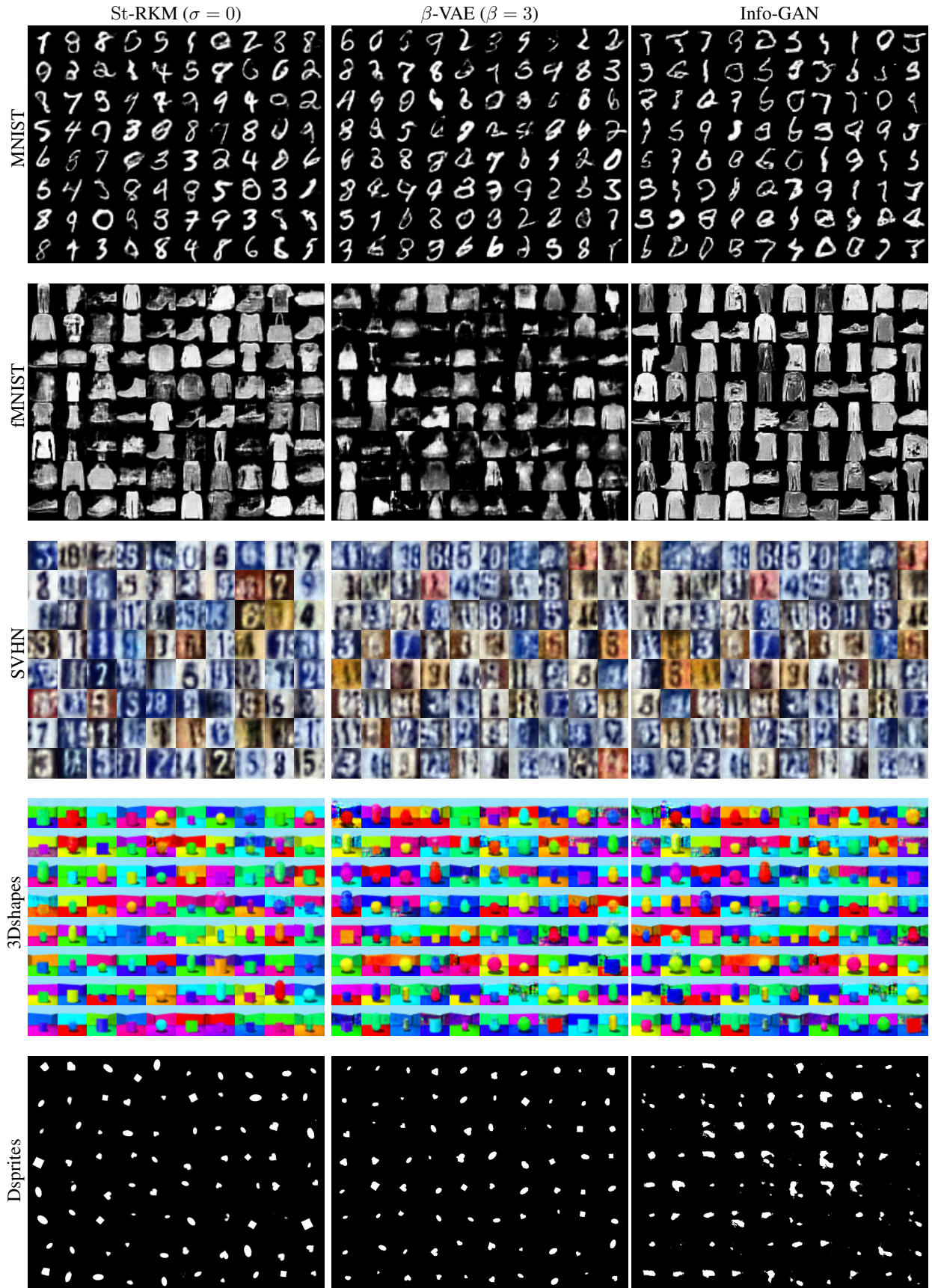


Figure 6: Samples of randomly generated batch of images to compute FID scores (see Table 1) and SWD scores (see Table 6).

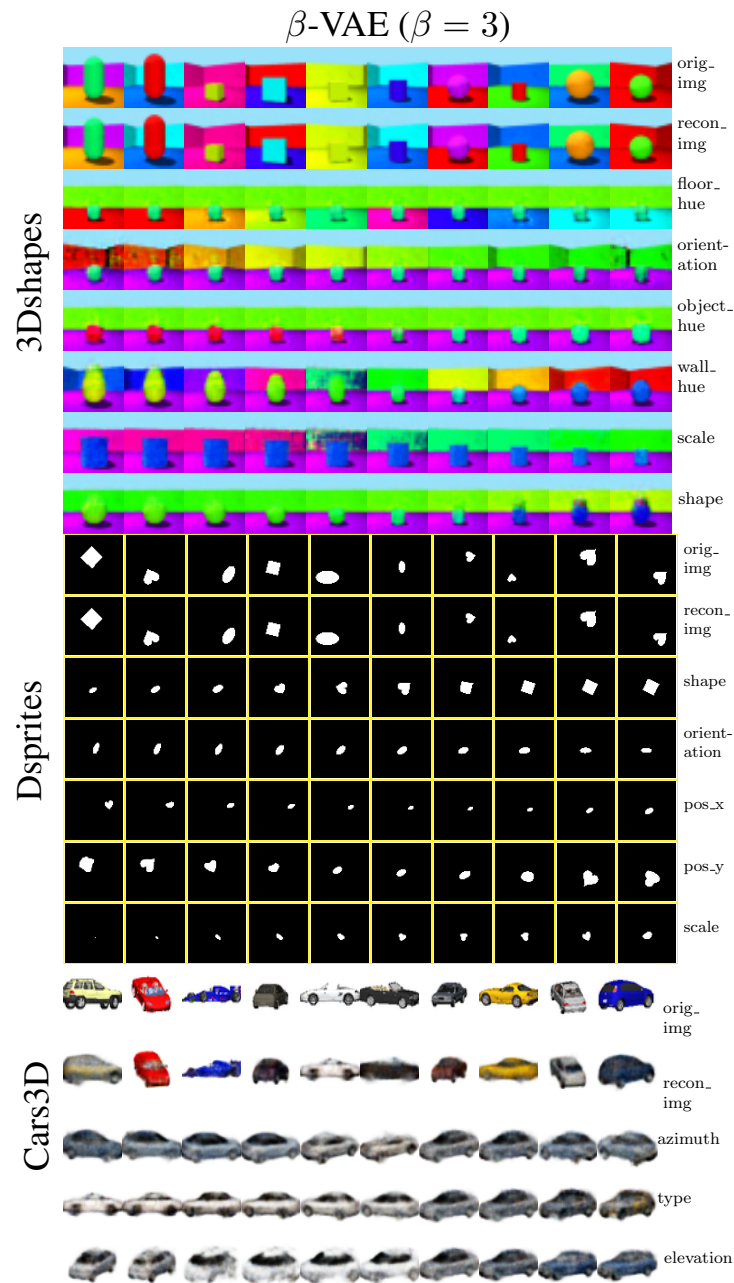


Figure 7: β -VAE: Traversals along principal components. First-two rows show the ground-truth and reconstructed images and each subsequent row shows the generated images by traversing along a principal component in the latent space. The last column in each images shows the dominant factor of variation.